Inorganic Chemistry

Article

pubs.acs.org/IC

Analysis of the Bonding between Two M(μ-NAr$^{\#}$) Monomers in the Dimeric Metal(II) Imido Complexes {M(μ-NAr$^{\#}$)}$_2$ [M = Si, Ge, Sn, Pb; Ar$^{\#}$ = C_6H_3-2,6-(C_6H_2-2,4,6-R_3)$_2$]. The Stabilizing Role Played by R = Me and iPr

Mateusz Brela,[†,‡] Artur Michalak,[‡] Philip P. Power,[§] and Tom Ziegler*[,†]

[†]Department of Chemistry, University of Calgary, 2500 University Drive NW, T2N 1N4 Calgary, Alberta, Canada

[‡]Department of Theoretical Chemistry, Faculty of Chemistry, Jagiellonian University, Ingardena 3, 30-060 Krakow, Poland

[§]Department of Chemistry, University of California, 1 Shields Avenue Davis, California 95616, United States

Supporting Information

ABSTRACT: The nature of the bonding between the two M(μ-NAr$^{\#}$) imido monomers [M = Si, Ge, Sn, Pb; Ar$^{\#}$ = C_6H_3-2,6-(C_6H_2-2,4,6-R_3)$_2$; R = Me, iPr] in the {M(μ-NAr$^{\#}$)}$_2$ dimer is investigated with the help of a newly developed energy and density decomposition scheme as well as molecular dynamics. The approach combines the extended transition state energy decomposition method with the natural orbitals for chemical valence density decomposition scheme within the same theoretical framework. The dimers are kept together by two σ bonds and two π bonds. The σ bonding has two major contributions. The first is a dative transfer of charge from nitrogen to M. It amounts to −188 kcal/mol for {Si(μ-NAr$^{\#}$)}$_2$, −152 kcal/mol for {Ge(μ-NAr$^{\#}$)}$_2$ with −105 kcal/mol for {Sn(μ-NAr$^{\#}$)}$_2$, and −79 kcal/mol for {Pb(μ-NAr$^{\#}$)}$_2$. The second is a charge buildup within the ring made up of the two dimers. It amounts to −82 kcal/mol for M = Si with −61 kcal/mol for M = Ge and ∼−50 kcal/mol for M = Sn and Pb. We finally have π bonding with a donation of charge from M to nitrogen. It has a modest contribution of ∼−30 kcal/mol. The presence of isopropyl (iPr) groups is further shown to stabilize{M(μ-NAr$^{\#}$)}$_2$ [M = Si, Ge, Sn, Pb; Ar$^{\#}$ = C_6H_3-2,6-(C_6H_2-2,4,6-iPr$_3$)$_2$] compared to the methylated derivatives (R = Me) through attractive van der Waals dispersion interactions.

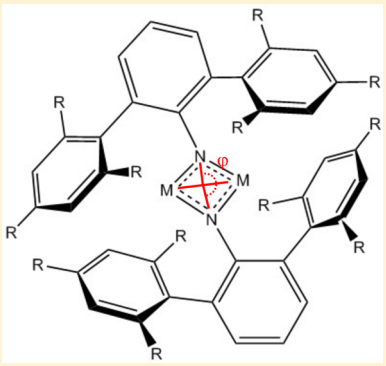

INTRODUCTION

Power et al. have recently synthesized the dimeric metal(II) imido complexes {M(μ-NAr$^{\#}$)}$_2$ [M = Ge, Sn, Pb; Ar$^{\#}$ = C_6H_3-2,6-(C_6H_2-2,4,6-Me_3)$_2$][1] as well as the isoelectronic phosphinidene[2] and thiolate[3] systems. Ghadwal et al. have recently prepared a stable dimer of the silaisonitrile compound and demonstrated that it has a planar core (N−Si−Si−N).[4] The dimeric imido molecules are isostructural and possess a nonplanar core (N−M−M−N) for M = Ge, Sn, and Pb. The bend along the M---M axes is ca. 173° for the germanium derivatives and ca. 149° for the tin and lead compounds. The smaller bending angle in the heavier homologues might potentially allow for stabilization of M−Ph interactions between the metal centers and flanking aryl rings. It has further been suggested that the electron-donating methyl (Me) or isopropyl (iPr) substituents on the aryl rings might help to stabilize the M−N bond electronically. It is the objective of the present study to probe the strength and nature of the bonds between the monomers in the dimer structure as well as the aryl ring−metal center interaction with the help of the extended transition state (ETS) energy decomposition scheme and the natural orbitals for chemical valence (NOCV) density decomposition approach. These techniques have recently been combined into the ETS−NOCV method and successfully applied to a number of problems involving bond analysis in inorganic complexes.[5−9] They include multiple bonds between transition metals[5] and main-group elements[6] as well as hydrogen and agnostic bonds.[9] A detailed description of the method has been given previously.[9]

We shall further assess whether Ar$^{\#}$ is able electronically to stabilize the dimeric structure either by electron donation from the iPr or Me substituents on the aryl rings or through dispersive van der Waals attractions between the two Ar$^{\#}$ ligands and their substituents on different metals. We shall finally study the factors responsible for the decrease in the bending angle from M = Ge to M = Sn and Pb by combining ab initio molecular dynamics with the ETS−NOCV method.

COMPUTATIONAL METHODS AND DETAILS

ETS Method. The bonding between two monomers in the dimeric structures was analyzed with the ETS bond energy decomposition scheme.[7−9] In this approach, the overall bonding energy is decomposed as shown in eq 1.

Received: December 20, 2013
Published: February 6, 2014

   dx.doi.org/10.1021/ic403108z | Inorg. Chem. 2014, 53, 2325−2332

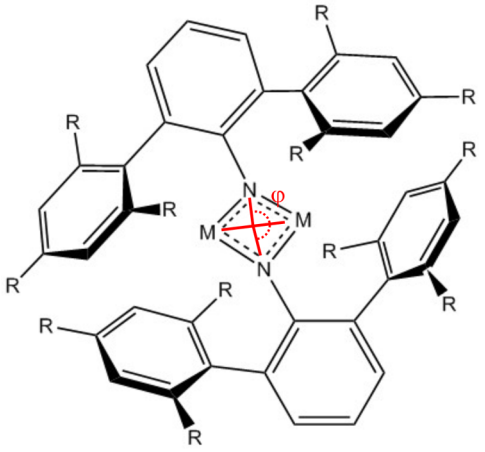

Figure 1. Structure of the studied dimers. R = Me and iPr; M = Si, Ge, Sn, and Pb.

$$\Delta E_{\text{total}} = \Delta E_{\text{dist}} + \Delta E_{\text{elstat}} + \Delta E_{\text{Pauli}} + \Delta E_{\text{disp}} + \Delta E_{\text{orb}} \quad (1)$$

Here ΔE_{dist} is the energy required to distort the geometry of the two monomers to the geometry that they take up in the dimer. The ΔE_{elstat} term is the electrostatic interaction between the frozen charge distributions of the two distorted monomers (fragments) as they are brought together. Further, ΔE_{Pauli} is the repulsive interaction between occupied orbitals on the two monomers, whereas ΔE_{disp} is the stabilizing dispersion interaction between the two fragments. Further, we allow the virtual orbitals on both monomers in the dimeric structure to participate in the bonding, leading to the orbital stabilization term ΔE_{orb}. Participation of the virtual orbitals gives rise to a change in the density, $\Delta\rho$. It is convenient to combine ΔE_{elstat} and ΔE_{Pauli} into the steric interaction energy as

$$\Delta E_{\text{steric}} = \Delta E_{\text{elstat}} + \Delta E_{\text{Pauli}} \quad (2)$$

NOCV. Historically, NOCV[10,11] has been extracted from the Nalewajski–Mrozek valence theory[12,13] as the eigenvectors that diagonalize the deformation density matrix. It was shown that the NOCV pairs (ψ_{-k}, ψ_k) decompose the deformation density $\Delta\rho$ into NOCV contributions $(\Delta\rho_k)$:

$$\Delta\rho(r) = \sum_{k=1}^{M/2} \nu_k[-\psi_{-k}^2(r) + \psi_k^2(r)] = \sum_{k=1}^{M/2} \Delta\rho_k(r) \quad (3)$$

where ν_k and M stand for the NOCV eigenvalues and the number of basis functions, respectively.

Visualization of the deformation density $(\Delta\rho_k)$ provides us with information about the direction of the charge flow. Thus, negative values of $\Delta\rho_k$ represent depletion and positive values accumulation.

ETS–NOCV Scheme. In the combined ETS–NOCV scheme, the orbital interaction contribution (ΔE_{orb}) is expressed in terms of NOCVs and their eigenvalues (ν_k), as shown in eq 4.

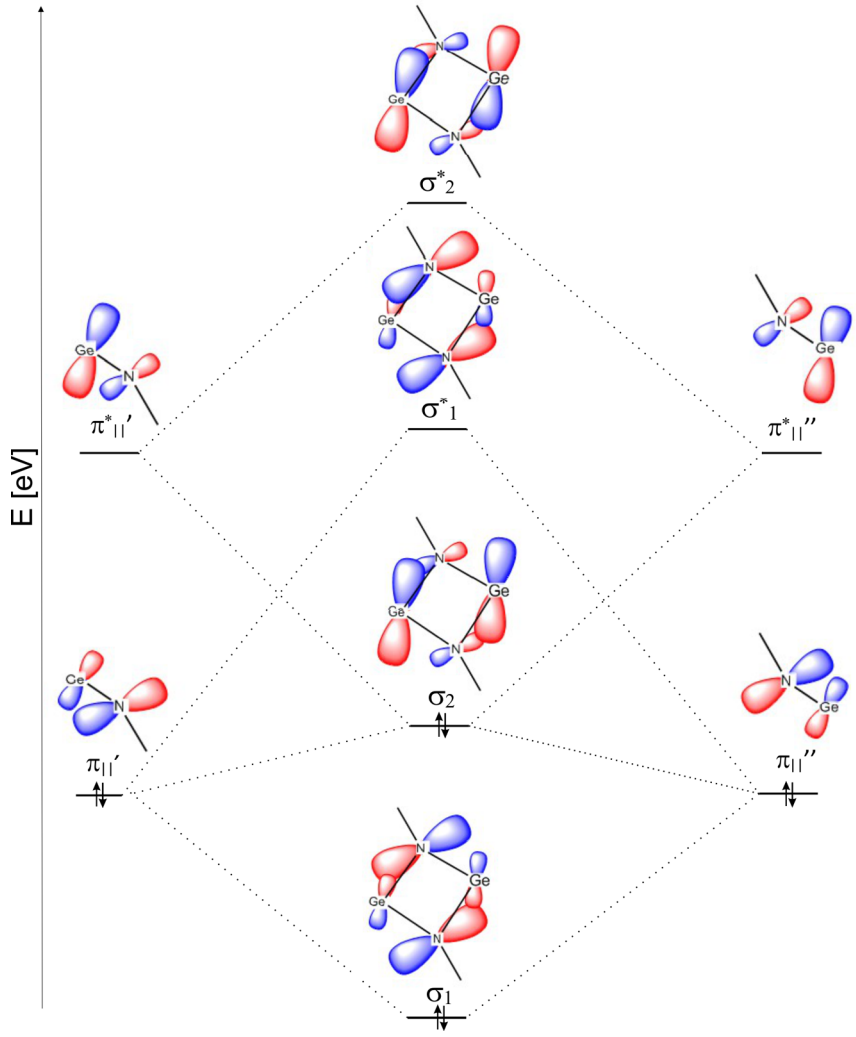

Figure 2. Key molecular orbitals of $\{M(\mu\text{-}NAr^{\#})\}_2$ involved in σ bonding.

dx.doi.org/10.1021/ic403108z | Inorg. Chem. 2014, 53, 2325–2332

$$\Delta E_{orb} = \sum_{k} \Delta E^{k}_{orb} = \sum_{k=1}^{M/2} \nu_k[-F^{TS}_{-k,-k} + F^{TS}_{k,k}] \quad (4)$$

Here $F^{TS}_{i,i}$ are diagonal Kohn–Sham matrix[14] elements defined over NOCVs with respect to the transition state (TS) density (at the midpoint between the density of the molecule and the sum of the fragment densities). The components ΔE^{k}_{orb} provide the energy associated with the change in density, $\Delta\rho_k$.

Computational Details. All density functional theory (DFT) static calculations presented here were based on the *Amsterdam Density Functional (ADF)* program version 2013.01 in which the ETS–NOCV scheme was implemented.[15] Use was made of the Becke–Perdew exchange-correlation functional[16,17] together with the dispersion correction scheme by Grimme et al.[18] A standard triple-ζ STO basis set with one set of polarization functions was used for all atoms. The relativistic effects for the heavy atoms (Ge, Sn, and Pb) were included at the scalar relativistic ZORA[19,20] level of approximations, as implemented in the *ADF* package.

Our ab initio DFT Born–Oppenheimer molecular dynamics (BOMD) simulations employed the *CP2K* package.[21−23] The 30 ps trajectory for the dimer structures was based on the exchange-correlation functional by Lee et al.[24] with Grimme's dispersion corrections.[18] A mixture of a DZVP basis sets and plane waves (cutoff = 260) were used. The time step was 0.5 fs. All dynamics calculations were performed with an NVT ensemble (353 K) controlled by a Nose-Hoover chain thermostat. A 5 ps equilibration was needed to stabilize the temperature with the thermostat. The trajectory was analyzed with the *VMD* package.[25]

Molecular Models. We studied the three imide dimers with the formula $\{M(\mu\text{-}NAr^{\#})\}_2$ [M = Si, Ge, Sn, Pb; $Ar^{\#} = C_6H_3\text{-}2,6\text{-}(C_6H_2\text{-}2,4,6\text{-}Me_3)_2$]. Crystal structures were available for these compounds, and they were used as the starting point for geometry optimization. The study of the influence of dispersion was performed by including not-yet-isolated isopropyl derivatives [M = Si, Ge, Sn, Pb; $Ar^{\#} = C_6H_3\text{-}2,6\text{-}(C_6H_2\text{-}2,4,6\text{-}iPr)_2$] in our computational study. A structure is shown in Figure 1.

RESULTS AND DISCUSSION

Fragment and Molecular Orbitals. In any discussion of bonding, one is required to specify the species (fragments) between which the bond is formed. In NOCV analysis, we consider the compounds $\{M(\mu\text{-}NAr^{\#})\}_2$ [M = Si, Ge, Sn, Pb; $Ar^{\#} = C_6H_3\text{-}2,6\text{-}(C_6H_2\text{-}2,4,6\text{-}Me_3)_2$], as formed from two $M(\mu\text{-}NAr^{\#})$ units. Thus, we are here looking for the bonds formed between the two monomers in a dimerization process. Each fragment has two occupied π orbitals designated as $\pi_{\parallel}$ and $\pi_{\perp}$ that are polarized toward nitrogen as well as two empty π^* orbitals, $\pi_{\parallel}^*$ and $\pi_{\perp}^*$, polarized toward the metal. It follows from Figure 2 that $\pi_{\parallel}'$ and $\pi_{\parallel}''$ form the occupied in-phase σ-bonding dimer orbital σ_1 as well as the empty out-of-phase σ_1^* orbital. On the other hand, $\pi_{\parallel}^{*\prime}$ and $\pi_{\parallel}^{*\prime\prime}$ give rise to the occupied bonding combination σ_2 and the empty antibonding orbitals σ_2^*. Thus, as the two new N–M σ bonds are formed, the density is transferred from $\pi_{\parallel}$ to $\pi_{\parallel}^*$ on the two fragments. Contour plots of σ_1, σ_2, σ_1^*, and σ_2^* are shown for M = Ge in the Supporting Information (SI).

In Figure 3, we depict the π-bond formation between the two monomers. Thus, the stabilizing interactions between $\pi_{\perp}'$ and $\pi_{\perp}''$ result in the bonding orbital π_1 with the largest lobes on the nitrogen atom. The corresponding antibonding interaction between $\pi_{\perp}'$ and $\pi_{\perp}''$ results in an out-of-phase interaction between the nitrogen and metal on different fragments. However, this interaction can be reduced by the admixture of the in-phase combination between $\pi_{\perp}^{*\prime}$ and $\pi_{\perp}^{*\prime\prime}$ to finally form the nonbonding and occupied orbital π_2 with two large lobes on nitrogen, as shown in Figure 3. Thus, the π bonding

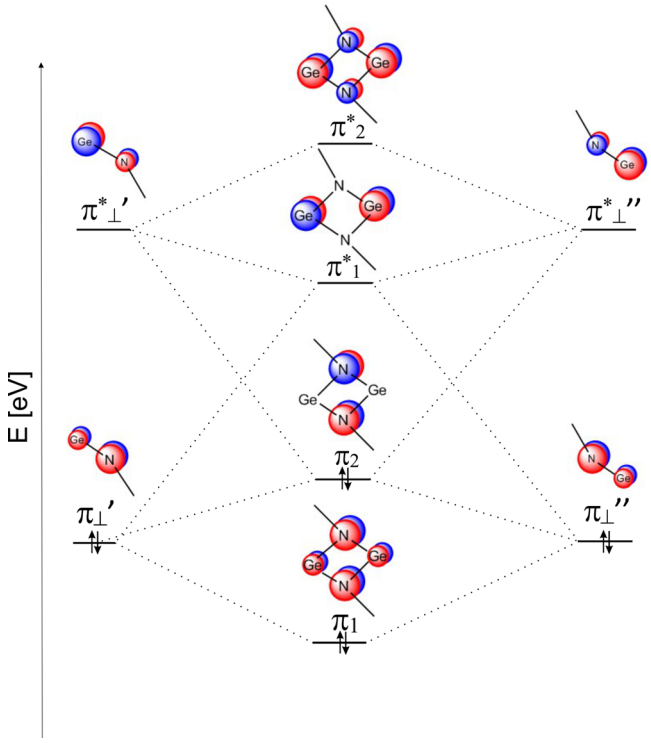

Figure 3. Key molecular orbitals of $\{M(\mu\text{-}NAr^{\#})\}_2$ involved in π bonding.

involves a transfer of charge from the metal to nitrogen due to the contribution from $\pi_{\perp}^{*\prime}$ and $\pi_{\perp}^{*\prime\prime}$ to π_2. Contours of the dimer π orbitals are shown in the SI.

NOCV–ETS Analysis of the Dimeric Compounds Based on the Monomers. Table 1 affords ETS analysis of the bonds formed between two $M(\mu\text{-}NAr^{\#})$ units. The steric term represents the total destabilizing interaction of the occupied orbitals on the two fragments. It is usually positive when we, as in the case here, are dealing with neutral fragments and ranges from 82.5 kcal/mol (Pb) to 234.4 kcal/mol (Si). The second destabilizing factor, ΔE_{dist}, is related to the geometry change on going from the optimized geometries of the free monomers to the structures of the monomers linked in the dimer. ΔE_{dist} has contributions from 27.15 kcal/mol (Pb) to 44.8 kcal/mol (Si). The larger part of ΔE_{dist} is connected to an increase in the M–N distance upon dimerization. The increases are 0.32 Å (Si), 0.25 Å (Ge), and 0.24 Å (Sn and Pb). A significant difference in the M–N–$Ar^{\#}$ angle has been observed. The angle decreased from 177° (optimized monomer) to 133° (dimer) for Si, from 173° to 133° for Ge, from 164° to 128° for Sn, and from 147° to 126° for Pb. The van der Waals dispersion ΔE_{disp} is significant and stabilizes the dimer, with contributions between −20.0 kcal/mol (Sn) and −24.5 kcal/mol (Pb). A large part of ΔE_{disp} comes from the van der Waals interactions between methyl groups on different fragments. Stable $\{M(\mu\text{-}NAr^{\#})\}_2$ compounds often contain alkyl (methyl) groups, and it is thus clear from our analysis that one of the roles played by the alkyl (methyl) groups is to stabilize the $\{M(\mu\text{-}NAr^{\#})\}_2$ dimer through ΔE_{disp}.

The factor of largest importance for the dimer stability is ΔE_{orb} (Table 1). It is more stabilizing for silicon (−309.1 kcal/mol) than for germanium (−246.0 kcal/mol) and tin (−186.9 kcal/mol) or lead (−157.5 kcal/mol). This is not surprising because the bonding overlaps between orbitals on different

dx.doi.org/10.1021/ic403108z | Inorg. Chem. 2014, 53, 2325−2332

Table 1. ETS Analysis[a] for the Dimeric Metal(II) Imido Complexes $\{M(\mu\text{-}NAr^{\#})\}_2$ [M = Si, Ge, Sn, Pb; $Ar^{\#} = C_6H_3\text{-}2,6\text{-}(C_6H_2\text{-}2,4,6\text{-}Me_3)_2$] Using BP86(D3)

M	ΔE_{Pauli}	ΔE_{elstat}	ΔE_{steric}[b]	ΔE_{orb}	ΔE_{disp}	ΔE_{dist}	ΔE_{total}[a]
Si	525.87	−291.48	234.39	−309.06	−22.81	44.82	−52.67
Ge	439.83	−261.81	178.02	−246.03	−22.52	35.72	−54.81
Sn	342.72	−233.15	109.57	−186.90	−20.04	30.97	−66.40
Pb	295.18	−212.68	82.50	−157.50	−24.48	27.15	−72.33

[a]Total bonding energy: $\Delta E_{total} = \Delta E_{steric} + \Delta E_{orb} + \Delta E_{disp} + \Delta E_{dist}$. [b]Steric interaction: $\Delta E_{steric} = \Delta E_{Pauli} + \Delta E_{elstat}$. [c]Energies in kcal/mol.

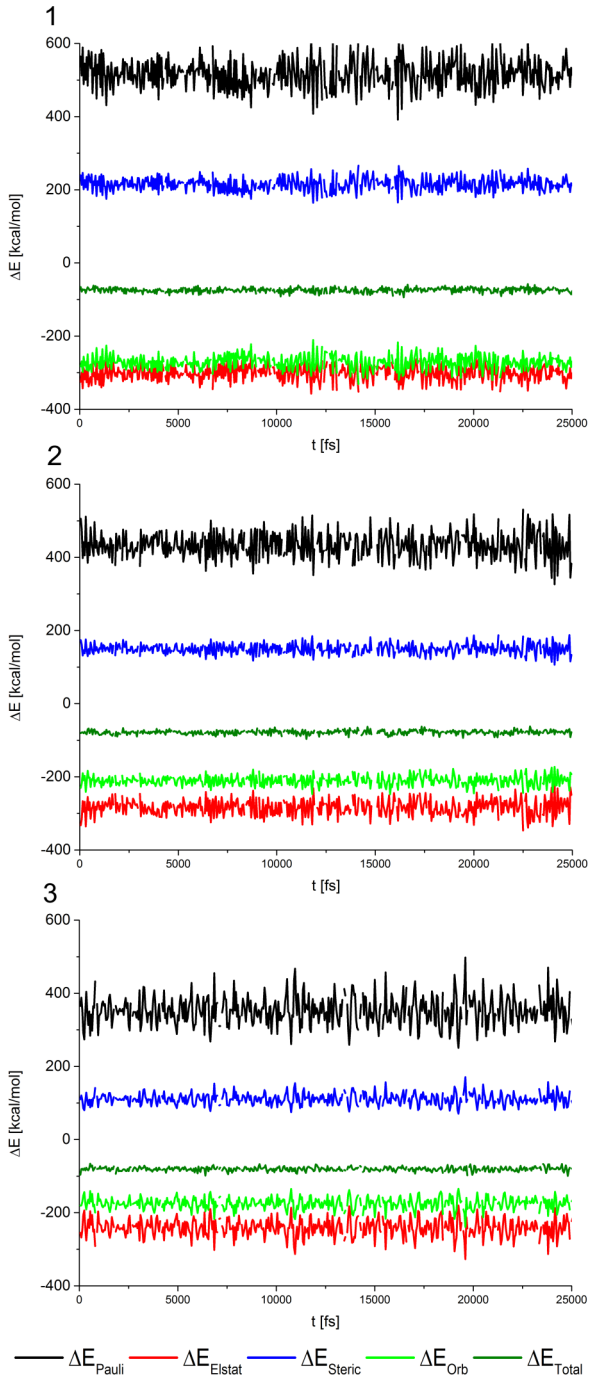

Figure 4. Change in the ETS components with time from a molecular dynamics simulations: (1) $\{Ge(\mu\text{-}NAr^{\#})\}_2$; (2) $\{Sn(\mu\text{-}NAr^{\#})\}_2$; (3) $\{Pb(\mu\text{-}NAr^{\#})\}_2$. Total bonding energy: $\Delta E_{total} = \Delta E_{steric} + \Delta E_{orb} + \Delta E_{disp}$.

Table 2. NOCV Analysis[a] for the Dimeric Metal(II) Imido Complexes $\{M(\mu\text{-}NAr^{\#})\}_2$ [M = Si, Ge, Sn, Pb; $Ar^{\#} = C_6H_3\text{-}2,6\text{-}(C_6H_2\text{-}2,4,6\text{-}Me_3)_2$] Using BP86(D3) (Energies in kcal/mol)

M	ΔE^1_{orb}	ΔE^2_{orb}	ΔE^{rest}_{orb}
Si	−188.37	−38.19	−82.50
Ge	−151.88	−32.99	−61.16
Sn	−104.92	−30.67	−51.30
Pb	−78.79	−29.44	−49.27

[a]See Figure 5. $\Delta E_{orb} = \Delta E^1_{orb} + \Delta E^2_{orb} + \Delta E^{rest}_{orb}$. Here $\Delta E^1_{orb} = \Delta E^{\sigma}_{orb}$ and $\Delta E^2_{orb} = \Delta E^{\pi}_{orb}$.

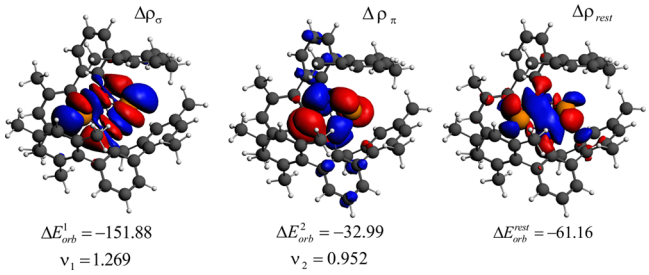

Figure 5. NOCV deformation densities for methylated $\{Ge(\mu\text{-}NAr^{\#})\}_2$ based on the monomeric fragment $Ge(\mu\text{-}NAr^{\#})$. Contours of the NOCV deformation density with the corresponding energy contributions. The contour values are 0.003 au. Energies are in kilocalories per mole. Blue represents density accumulation and red density depletion.

fragments decrease from silicon to lead. The total interaction energy is, according to eqs 1 and 2, the sum of the steric interaction energy term, the orbital interaction contribution, the van der Waals dispersion stabilization, and the distortion energy. It is important to note that the lead compound has the most stabilizing interaction energy with ΔE_{total} = −72.3 kcal/mol as a result of the weaker steric repulsion. On the other hand, for the other dimers ΔE_{total} decreases gradually in absolute terms as −66.4 kcal/mol (Sn) and −54.8 kcal/mol (Ge) or −52.7 kcal/mol (Si). It follows from Table 3 that the steric interaction decreases down the series from M = Si to Pb as the repulsive interaction between aryl groups on different fragments diminishes with longer N−M distances.

We have carried out BOMD simulations on each dimer to monitor how their structures evolve with time at room temperature. By performing ETS−NOCV analyses for each time step (snapshot), we are thus able to monitor how each ETS−NOCV component changes as a result of the nuclear thermal motion (see Figure 4). Thermal motion over time changes the steric interaction energy ΔE_{steric} by as much as 200 kcal/mol for each molecule, and the frequency of change is different. The fastest changes are observed for the germanium dimer and the slowest for the lead compound. This trend is observed for all contributions. The effect can be connected to a

dx.doi.org/10.1021/ic403108z | Inorg. Chem. 2014, 53, 2325−2332

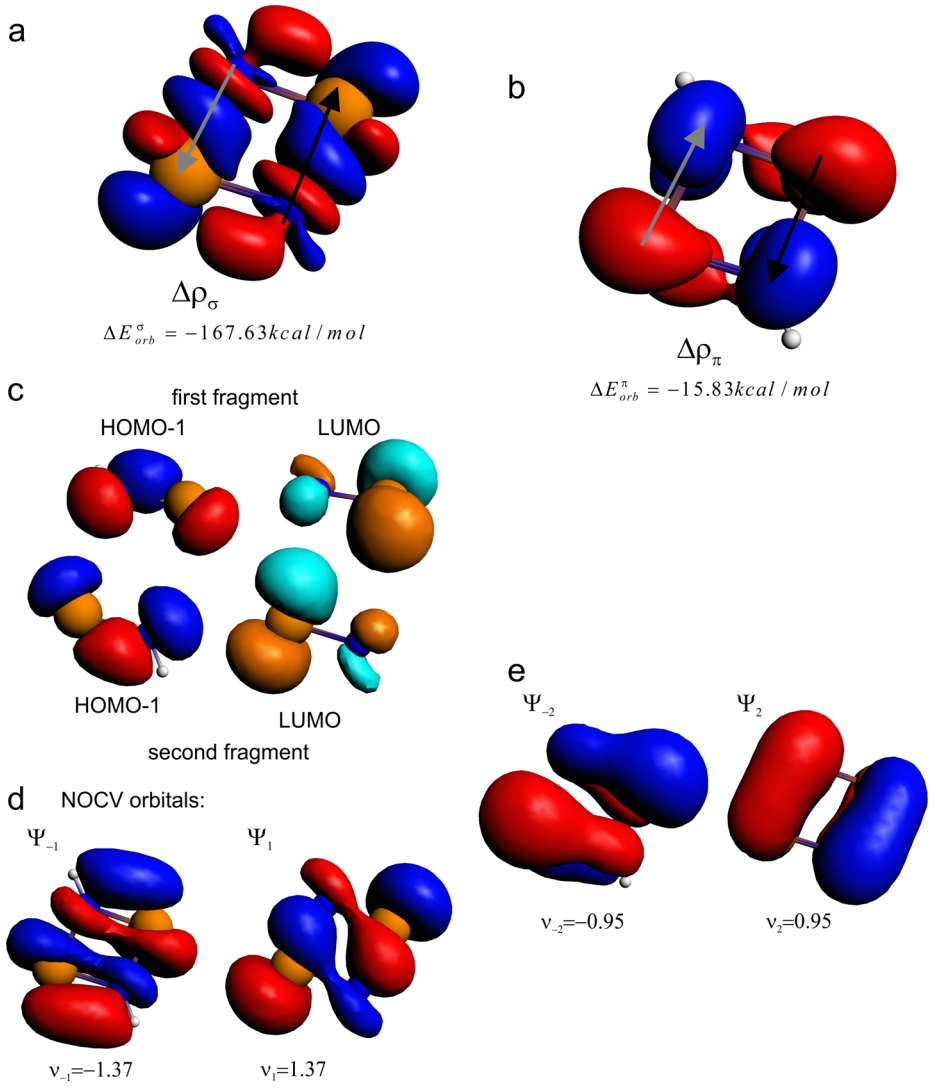

Figure 6. Interpretation of the first two NOCV channels based on the model system: $\{GeNH\}_2$. Parts a and b show the deformation densities $\Delta\rho_\sigma$ and $\Delta\rho_\pi$, respectively. The center panel presents combinations of the occupied and virtual fragment orbitals involved in charge transfer, leading to $\Delta\rho_\sigma$. The bottom panel shows the corresponding NOCV orbitals with eigenvalues corresponding to $\Delta\rho_\sigma$ (d) and $\Delta\rho_\pi$ (e).

difference in atomic masses of M and the strength of the N−M bonds. It should be pointed out that all BOMD results are fully consistent with the finding from our static calculations as far as the relative importance of the different contributions are concerned.

In Table 2, we provide NOCV decomposition of ΔE_{orb} based on the BP86 functional for M = Si, Ge, Sn, and Pb according to

$$\Delta E_{orb} = \Delta E^1_{orb} + \Delta E^2_{orb} + \Delta E^{rest}_{orb} \quad (5)$$

The first two NOCV energy contributions to ΔE_{orb} are shown as ΔE^1_{orb} and ΔE^2_{orb}, respectively, in Table 2. Here ΔE^1_{orb} dominates, with values ranging from −188.4 kcal/mol for Si to −78.8 kcal/mol for Pb. The corresponding density contributions indicate that ΔE^1_{orb} represents formation of the σ_2-bonding orbital in Figure 2. It is shown as $\Delta\rho_\sigma$ in Figure 5 for $\{Ge(\mu\text{-}NAr^{\#})\}_2$, and we observe clearly a flow of density from nitrogen to metal in accordance with charge transfer from $\pi_\parallel$ to $\pi_\parallel{}^*$ in Figure 2.

Further analysis is provided in Figure 6, where we for clarity have used $\{Ge(\mu\text{-}NH)\}_2$ as a model. In $\Delta E^1_{orb} = \Delta\rho_\sigma$ of Figure 6a, density is transferred from ψ_{-1} to ψ_1 of Figure 6d. Here ψ_{-1} is identified as the out-of-phase combination of $\pi_\parallel{}'$ and $\pi_\parallel{}''$ also shown in Figure 6c, whereas ψ_1 corresponds to the in-phase combination between $\pi_\parallel{}^{*\prime}$ and $\pi_\parallel{}^{*\prime\prime}$. This is in line with our molecular orbital analysis in Figure 2 where ψ_{-1} is identical with $\sigma_1{}^*$ and ψ_1 corresponds to σ_2. Figure 6a illustrates that $\Delta\rho_\sigma$ of the model compound is qualitatively similar to that of the real systems shown in Figure 5. The dimerization process is formally a symmetry-forbidden 2 + 2 cycloaddition. Thus, at large interfragment distances, the out-of-phase combination of $\pi_\parallel{}'$ and $\pi_\parallel{}''$, called $\sigma_1{}^*$, is occupied. However, as the fragments approach, the antibonding interaction between $\pi_\parallel{}'$ and $\pi_\parallel{}''$ increases and charge is transferred to the in-phase combination between $\pi_\parallel{}^{*\prime}$ and $\pi_\parallel{}^{*\prime\prime}$, called σ_2, which is unoccupied in the free fragments.

The second contribution ΔE^2_{orb} is numerically much smaller and amounts to −38.2 kcal/mol for M = Si and −29.4 kcal/mol for M = Pb (see Table 2). It follows from $\Delta\rho_\pi$ of Figure 5 that it represents the π bonds formed between the two N−M units of the dimer. As discussed in connection with Figure 3, the π-bond formation shown involves (back) donation from metal to nitrogen. This is clearly seen to be the case from the plot of $\Delta\rho_\pi$ in Figure 3.

dx.doi.org/10.1021/ic403108z | Inorg. Chem. 2014, 53, 2325−2332

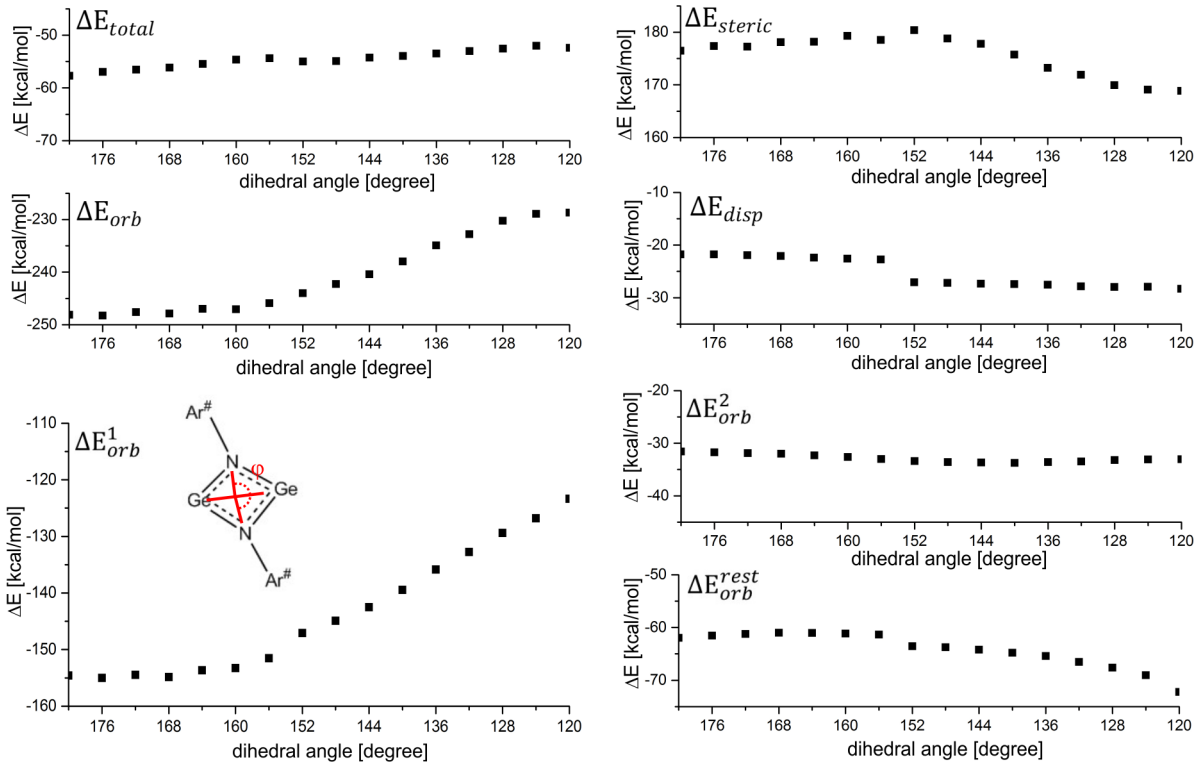

Figure 7. Top four charts presenting different components from ETS analysis of the dimeric metal(II) imido complex $\{M(\mu\text{-}NAr^{\#})\}_2$ [M = Ge; $Ar^{\#}$ = C_6H_3-2,6-(C_6H_2-2,4,6-Me_3)$_2$] as a function of the dihedral angle N−Ge−Ge−N, φ, using BP86(D3). Three bottom charts showing the contribution to ΔE_{orb} from the three NOCV components $\Delta\rho_1$, $\Delta\rho_2$, and $\Delta\rho_{rest}$ as a function of φ. Here $\Delta E^1_{orb} = \Delta E^{\sigma}_{orb}$, and $\Delta E^2_{orb} = \Delta E^{\pi}_{orb}$.

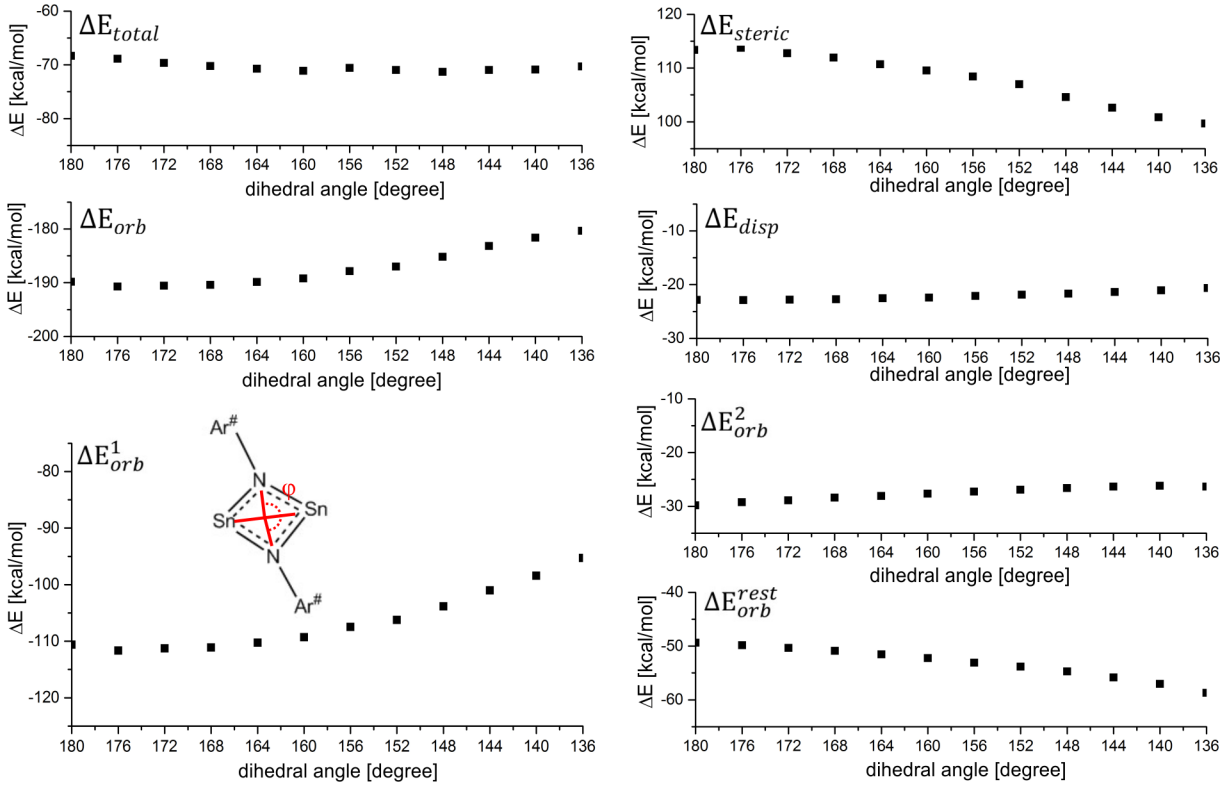

Figure 8. Top four charts presenting different components from ETS analysis of the dimeric metal(II) imido complex $\{M(\mu\text{-}NAr^{\#})\}_2$ [M = Sn; $Ar^{\#}$ = C_6H_3-2,6-(C_6H_2-2,4,6-Me_3)$_2$] as a function of the dihedral angle N−Sn−Sn−N, φ, using BP86(D3). Three bottom charts showing the contribution to ΔE_{orb} from the three NOCV components $\Delta\rho_1$, $\Delta\rho_2$, and $\Delta\rho_{rest}$ as a function of φ. Here $\Delta E^1_{orb} = \Delta E^{\sigma}_{orb}$, and $\Delta E^2_{orb} = \Delta E^{\pi}_{orb}$.

dx.doi.org/10.1021/ic403108z | Inorg. Chem. 2014, 53, 2325−2332

Table 3. ETS Analysis for the Dimeric Metal(II) Imido Complexes $\{M(\mu\text{-}NAr^{\#})\}_2$ [M = Si, Ge, Sn, Pb; $Ar^{\#} = C_6H_3\text{-}2,6\text{-}(C_6H_2\text{-}2,4,6\text{-}iPr_3)_2$] Using BP86(D3)

system	ΔE_{Pauli}	ΔE_{elstat}	ΔE_{steric} [b]	ΔE_{orb}	ΔE_{disp}	ΔE_{dist}	ΔE_{total} [a]
Si−iPr	564.85	−305.45	259.40	−320.19	−49.74	51.22	−59.30
Ge−iPr	470.85	−271.10	199.75	−256.80	−49.12	44.65	−61.52
Sn−iPr	375.22	−243.56	131.66	−195.61	−44.61	37.78	−70.78
Pb−iPr	314.13	−217.83	96.30	−161.46	−46.00	32.12	−79.05

[a]Total bonding energy: $\Delta E_{total} = \Delta E_{steric} + \Delta E_{orb} + \Delta E_{disp} + \Delta E_{dist}$, [b]Steric interaction: $\Delta E_{steric} = \Delta E_{Pauli} + \Delta E_{elstat}$. [c]Energies in kcal/mol.

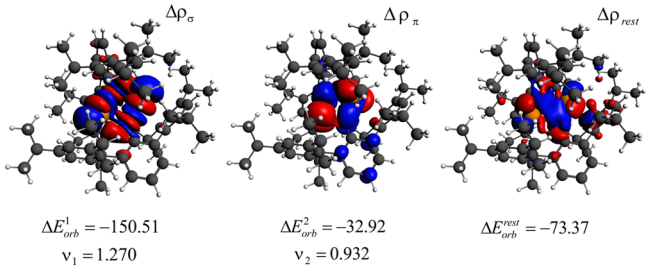

Figure 9. NOCV deformation densities for isopropylated $\{Ge(\mu\text{-}NAr^{\#})\}_2$ based on the monomeric fragment $Ge(\mu\text{-}NAr^{\#})$. Contours of the NOCV deformation density with the corresponding energy contributions. The contour values are 0.003 au. Energies are in kilocalories per mole. Blue represents density accumulation and red density depletion.

The remaining part of the orbital interaction is marked in Table 2 as ΔE^{rest}_{orb}. It amounts to −82.5 kcal/mol for M = Si and −49.3 kcal/mol for M = Pb and comes from six contributions ΔE^{n}_{orb} (n = 3 and 8) of decreasing magnitude, as shown in Figure SI4 in the SI. We depict $\Delta\rho_{rest}$ in Figure 5. It represents a charge buildup within the $(M-N)_2$ ring made up of the two monomers. It can to a large extent be associated with formation of the σ_1 bonding orbital in Figure 2 and must as such be considered a second contribution to the σ-bond formation.

NOCV−ETS Analysis of the Factors Influencing the Planarity of the $(M-N)_2$ Core in the Dimeric Structure. Figure 7 displays the ETS−NOCV analysis for the germanium compound as a function of the N−M−M−N dihedral angle φ (marked on Figures 1, 7, and 8). A 180° dihedral angle corresponds to the planar system. It is clear from the ΔE_{total} chart (left top panel) that the energy of the germanium system has a minimum close to φ = 180°. This minimum for germanium is due to ΔE^{1}_{orb}, whereas ΔE_{steric} would prefer a bent structure. The same factors are responsible for the completely planar structure for M = Si. For the lead and tin systems, we observed a preference for the geometry with $\varphi \sim 140°$. Figure 8 depicts decomposition for the tin compound. The optimized structure ($\varphi \sim 140°$) is a compromise between ΔE_{orb}, which prefers a planar system, and ΔE_{steric}, for which a nonplanar system is preferred. The dispersion contribution ΔE_{disp} has little influence on the geometry for tin and lead. This is in contrast to M = Ge, where dispersion prefers the bent structure by 6 kcal/mol. In conclusion, for M = Si and Ge, the bonding interaction between orbitals on different fragments is strong because of the short interfragment M−N distance. Thus, any bending that would reduce this interaction is prohibitive in terms of energy, and the systems adopt a planar structure. For M = Sn and Pb, the bonding interactions are much weaker because of the longer M−N distances. Hence, a bending driven by a reduction in the steric interaction is possible, and the systems adopt a bent geometry.

Table 3 affords ETS analysis from dimerization of two $M(\mu\text{-}NAr^{\#})$ units containing isopropyl groups [M = Si, Ge, Sn, Pb; $Ar^{\#} = C_6H_3\text{-}2,6\text{-}(C_6H_2\text{-}2,4,6\text{-}iPr_3)_2$] rather than methyl. A comparison of Tables 1 and 3 reveals that ΔE_{disp} stabilization for R = iPr is roughly double that for R = Me, whereas ΔE_{orb} is increased from ∼10 kcal/mol primarily through ΔE^{rest}_{orb}. On the other hand, the steric repulsion, ΔE_{steric}, is enhanced, as expected. The enhancement amounts to −25 kcal/mol for Si and −20 kcal/mol for Ge and Sn compared to −15 kcal/mol for Pb. In the final analyses, we find that the dimerization energy, ΔE_{total}, has increased by 4 kcal/mol for tin and 5 kcal/mol for silicon compared to 7 kcal/mol for M = Ge and Pb. We note that M = Pb still has the largest dimerization energy. Figure 9 displays the deformation densities for $\Delta\rho_{\sigma}$, $\Delta\rho_{\pi}$, and $\Delta\rho_{rest}$ in the case of M = Ge and R = iPr. They are quite similar to those displayed in Figure 5 for R = Me. We found, in contrast to other dimers containing dimers of metal aryl monomers, little evidence from stabilizing interactions between a metal on one monomer and an aryl ring on another monomer.

CONCLUDING REMARKS

The present study affords a detailed analysis of the interactions between two monomeric units $M(\mu\text{-}NAr^{\#})$ in the dimeric metal(II) imido complexes $\{M(\mu\text{-}NAr^{\#})\}_2$ (M = Si, Ge, Sn, Pb). Analysis was carried out by employing the NOCV method together with the ETS scheme and molecular dynamics based on the Born−Oppenheimer approach (Table 4). In ETS−NOCV analysis, we consider $\{M(\mu\text{-}NAr^{\#})\}_2$ as formed from two $M(\mu\text{-}NAr^{\#})$ fragments with a singlet ground state. Our study revealed that σ bonding is more important than π bonding. For M = Si and Ge, the dimer prefers a planar structure with the dihedral M−N−N−M angle φ close to 180°. The planar structure is caused by the strong σ-bonding interaction ΔE^{1}_{orb}, whereas the steric interaction energy prefers a bent structure with φ < 180°. For M = Sn and Pb, the σ-bonding interaction ΔE^{1}_{orb} is reduced and ΔE_{steric} causes a bent structure with $\varphi \sim 149°$.

Table 4. NOCV Analysis for the Dimeric Metal(II) Imido Complexes $\{M(\mu\text{-}NAr^{\#})\}_2$ [M = Si, Ge, Sn, Pb; $Ar^{\#} = C_6H_3\text{-}2,6\text{-}(C_6H_2\text{-}2,4,6\text{-}iPr_3)_2$] Using BP86(D3) (Energies in kcal/mol)

M	ΔE^{1}_{orb}	ΔE^{2}_{orb}	ΔE^{rest}_{orb}
Si−iPr	−185.97	−38.93	−95.29
Ge−iPr	−150.51	−32.92	−73.37
Sn−iPr	−107.54	−28.18	−59.89
Pb−iPr	−75.75	−26.82	−58,89

[a]See Figure 9. $\Delta E_{orb} = \Delta E^{1}_{orb} + \Delta E^{2}_{orb} + \Delta E^{rest}_{orb}$. Here $\Delta E^{1}_{orb} = \Delta E^{\sigma}_{orb}$ and $\Delta E^{2}_{orb} = \Delta E^{\pi}_{orb}$.

dx.doi.org/10.1021/ic403108z | Inorg. Chem. 2014, 53, 2325−2332

Our analysis revealed further that the R substituents on the aryl groups (see Figure 1) have a stabilizing influence on the dimers through dispersive van der Waals attractions of R groups attached to aryl rings on different monomers. The stabilization amounted to ca. −20 kcal/mol for R = Me and ca. −45 kcal/mol for R = iPr. As a result, the dimerization energy ΔE_{total} is ∼4 kcal/mol larger for M = Sn, ∼5 kcal/mol larger for M = Si, and ∼7 kcal/mol larger for M = Ge and Pb despite of an increase in ΔE_{steric}. It was finally found that ΔE_{total} was larger for M = Pb than for M = Sn, Ge, and Si as a result of a more modest steric interaction energy that more than compensates for a decrease in ΔE_{orb} through the series M = Si, Ge, Sn, and Pb. Our study is an extension of the pioneering work by Ghadwal et al.[4] carried out for M = Si, where qualitative analysis established both σ and π bonding between the two monomers as well as a dimerization energy comparable to the one found here.

■ ASSOCIATED CONTENT

Supporting Information

Structures of considered systems (Figure S1), interpretation of the bonding molecular orbital as well as investigated fragment orbitals for $\{Pb(\mu\text{-}NAr^{\#})\}_2$ [$Ar^{\#}$ = C_6H_3-2,6-(C_6H_2-2,4,6-Me_3)$_2$; Figures S2 and S3], and contours of the NOCV deformation densities participating in ΔE_{orb}^{rest} for $\{Ge(\mu\text{-}NAr^{\#})\}_2$ [$Ar^{\#}$ = C_6H_3-2,6-(C_6H_2-2,4,6-Me_3)$_2$; Figure S4]. This material is available free of charge via the Internet at http://pubs.acs.org.

■ AUTHOR INFORMATION

Corresponding Author

*E-mail: ziegler@ucalgary.ca.

Notes

The authors declare no competing financial interest.

■ ACKNOWLEDGMENTS

T.Z. thanks the Canadian Government for a Canada Research Chair. M.B. acknowledges financial support from the International Ph.D. studies program at the Faculty of Chemistry, Jagiellonian University. This program was sponsored by the Foundation for Polish Science, cofinanced by the EU European Regional Development Fund. We are grateful for the allocation of CPU time on the "Zeus" supercomputer in Cracow. This research was supported by PL-Grid Infrastructure and resources provided by Academic Computational Center Cyfronet.

■ REFERENCES

(1) Merrill, W. A.; Wright, R. J.; Stanciu, C. S.; Olmstead, M. M.; Fettinger, J. C.; Power, P. P. *Inorg. Chem.* **2010**, *49*, 7097−7105.
(2) Merrill, Q. A.; Rivard, E.; DeRopp, J. S.; Wang, X.; Ellis, B. D.; Fettinger, J. C.; Wrackmeyer, B.; Power, P. P. *Inorg. Chem.* **2010**, *49*, 8481−8486.
(3) Rekken, B. D.; Brown, T. M.; Olmstead, M. M.; Fettinger, J. C.; Power, P. P. *Inorg. Chem.* **2013**, *52*, 3054−3062.
(4) Ghadwal, R. S.; Roesky, H. W.; Pröpper, K.; Dittrich, B.; Klein, S.; Frenking, G. *Angew. Chem., Int. Ed.* **2011**, *50*, 5374−5378.
(5) Ndambuki, S.; Ziegler, T. *Inorg. Chem.* **2012**, *51*, 7794−7800.
(6) Seidu, I.; Seth, M.; Ziegler, T. *Inorg. Chem.* **2013**, *52*, 8378−8388.
(7) Ziegler, T.; Rauk, A. *Theor. Chim. Acta* **1977**, *46*, 1−10.
(8) Ziegler, T.; Rauk, A. *Inorg. Chem.* **1979**, *18*, 1755−1759.
(9) Ziegler, T.; Rauk, A. *Inorg. Chem.* **1979**, *18*, 1558−1565.
(10) Michalak, A.; Mitoraj, M.; Ziegler, T. *J. Phys. Chem. A* **2008**, *112*, 1933−1939.
(11) Mitoraj, M.; Michalak, A.; Ziegler, T. J. *Chem. Theory Comput.* **2009**, *5*, 962−975.
(12) Nalewajski, R. F.; Mrozek, J. *Int. J. Quantum Chem.* **1996**, *57*, 377−389.
(13) Michalak, A.; De Kock, R.; Ziegler, T. *J. Phys. Chem. A* **2008**, *112*, 7256−7263.
(14) Koch, W.; Holthausen, M. C. *A Chemist's Guide to Density Functional Theory*; Wiley-VCH: New York, 2001.
(15) Te Velde, G.; Bickelhaupt, F. M.; Baerends, E. J.; van Gisbergen, S. J. A.; Guerra, C.; Snijders, J. G.; Ziegler, T. *J. Comput. Chem.* **2001**, *22*, 931−967.
(16) Becke, A. *Phys. Rev. B* **1988**, *38*, 3098−3100.
(17) Perdew, J. *Phys. Rev. B* **1986**, *33*, 8822−8824.
(18) Grimme, S.; Ehrlich, S.; Goerigk, L. *J. Comput. Chem.* **2011**, *32*, 1456−1465.
(19) van Lenthe, E.; Baerends, E. J.; Snijders, J. G. *J. Chem. Phys.* **1993**, *99*, 4597−4610.
(20) van Lenthe, E.; Baerends, E. J.; Snijders, J. G. *J. Chem. Phys.* **1994**, *101*, 9783−9792.
(21) VandeVondele, J.; Krack, M.; Mohamed, F.; Parrinello, M.; Chassaing, T.; Hutter, J. *Comput. Phys. Commun.* **2005**, *167*, 103−128.
(22) Krack, M.; Parrinello, M. *Forschungszentrum Jülich, NIC Ser.* **2004**, *25*, 29.
(23) VandeVondele, J.; Hutter, J. *J. Chem. Phys.* **2003**, *118*, 4365−4369.
(24) Lee, C.; Yang, W.; Parr, R. G. *Phys. Rev. B* **1988**, *37*, 785−789.
(25) Humphrey, W.; Dalke, A.; Schulten, K. *J. Mol. Graphics* **1996**, *14*, 33−38.